ACS APPLIED MATERIALS & INTERFACES

Research Article

www.acsami.org

Investigations into the Electrochemical, Surface, and Electrocatalytic Properties of the Surface-Immobilized Polyoxometalate, $TBA_3K[SiW_{10}O_{36}(PhPO)_2]$

Mustansara Yaqub,[†] Shahzad Imar,[†] Fathima Laffir,[‡] Gordon Armstrong,[‡] and Timothy McCormac*[,†]

[†]Electrochemistry Research Group, Department of Applied Science, Dundalk Institute of Technology, Dundalk, County Louth, Ireland

[‡]Materials and Surface Science Institute, University of Limerick Castletroy, County Limerick, Ireland

Supporting Information

ABSTRACT: Surface anchoring of an organic functionalized POM, $TBA_3K[SiW_{10}O_{36}(PhPO)_2]$ was carried out by two methods, the layer-by-layer (LBL) assembly technique by employing a pentaerythritol-based ruthenium(II) metallodendrimer as a cationic moiety and also by entrapping the POM in a conducting polypyrrole film. The redox behavior of the constructed films was studied by using cyclic voltammetry and electrochemical impedance spectroscopy. The surface morphologies of the constructed multilayers were examined by scanning electron microscopy and atomic force microscopy. X-ray photoelectron spectroscopy was conducted to confirm the elements present within the fabricated films. The multilayer assembly was also investigated for its catalytic efficiency towards the reduction of nitrite.

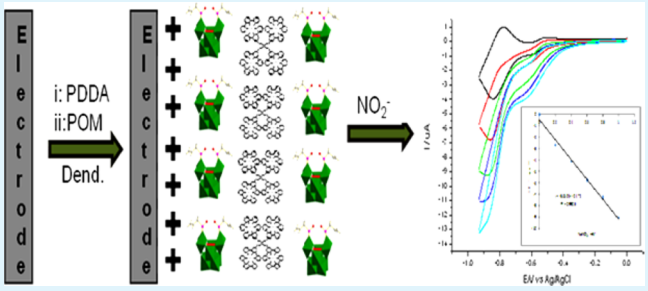

KEYWORDS: *polyoxometalate, polypyrrole, layer-by-layer, nitrite, electrocatalysis*

INTRODUCTION

Polyoxometalates (POMs) are inorganic metal-oxide aggregates that display great diversity in their structure and composition.[1,2] Their unmatched intrinsic properties render them promising candidates for use in areas such as biotechnology, material science, optics, magnetism, environmental sensing and medicine.[3−12] In a rapidly growing context of multifunctional molecular architectures, derivatized POMs constitute ideal building blocks owing to their enhanced stability and finely tuned electroactive properties. Among the several strategies to functionalize the POMs, while maintaining their intrinsic properties and structural integrity, the covalent attachment of organic moieties to the POM framework has many potential advantages as it provides a rational route to the modification of the electronic, magnetic, and optical characteristics of the POMs by an appropriate selection of the addenda atoms and organic groups,[13] for example, imido, silanes, or phosphonates. The most widely studied group of POMs are the Keggin type with the general formula $[XM_{12}O_{40}]^{n-}$ where M′ represents tungsten or molybdenum atoms while X is the heteroatom (X = P, Si, As, Ge). Bis-organophosphoryl decatungstosilicate, that is, $[SiW_{10}O_{36}(PhPO)_2]^{-4}$, a Keggin type polyoxometalate has been synthesized by the derivatization of a dilacunary anion, that is, $[SiW_{10}O_{36}]^{-8}$ with phenyl phosphonic acid. This dilacunary anion is highly neucleophilic and is formed by the removal of a tungsten−oxygen octahedral from a saturated Keggin structure $[XW_{12}O_{40}]^{n-}$.[14] The fully saturated organic−inorganic hybrid thus synthesized possesses virtual C_{2v} symmetry with two phenylphosphonate groups (PhPO) attached to two WO_6 octahedra of POM framework through their oxygen atoms as illustrated by Figure 1. This modified POM exhibits greater stability than its nonfunctionalized precursor, that is, $[\gamma\text{-}SiW_{10}O_{34}(H_2O)]^{-4}$.[15] Further more, this POM has been reported to exhibit excellent catalytic efficiency

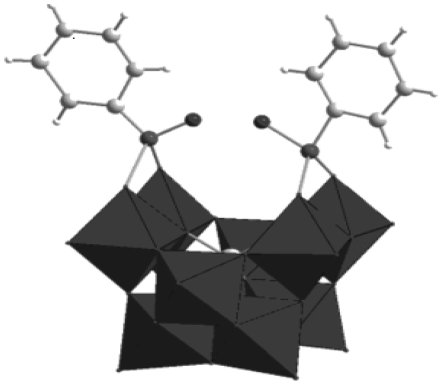

Figure 1. Polyhedra representation of $[TBA]_3K[SiW_{10}O_{36}(PhPO)_2]$.

Received: March 25, 2014
Accepted: December 5, 2014
Published: December 5, 2014

DOI: 10.1021/am5017864
ACS Appl. Mater. Interfaces 2015, 7, 1046−1056

towards the oxidation of alcohols and alkenes with almost ≥99% yield.[16]

Particular attention has been exercised toward the immobilization of POMs on different surfaces to achieve well-organized nanoassemblies with accessible redox states. Various techniques have been employed, such as, dip-coating, sol−gel technique, adsorption, Langmuir−Blodgett films, self-assembled monolayer,[17] electrodeposition, layer-by-layer assembly (LBL), and incorporation into conducting polymers.[18−21] LBL is believed to be the simplest and most effective method to develop well-ordered architectures with precisely controlled thicknesses resulting in films that exhibit excellent thermal, mechanical and chemical stabilities.[22−25] Previously, Cheng and co-workers[26] immobilized the phosphomolybdic acid POM on gold electrode by employing the LBL technique and investigated the electrocatalytic activity of the fabricated multilayer assembly toward the reduction of nitrite at very low pH that is, 0.5 M H_2SO_4. Multilayer assemblies of POM clusters with varying charges and sizes were prepared by Liu et al. to address the fundamental principles of this technique.[27] Cheng et al. also fabricated the multilayer nanoassemblies based on the Dawson type POM P_2W_{18}, and showed that the film exhibited catalytic response toward the reduction of iodate and oxidation of arsenite.[28]

POMs have been found to exhibit excellent electrocatalytic activity toward a variety of analytes, which is attributed to their ability to reversibly accept and donate electrons without any structural change. Nitrite occurs naturally and is an important element of the global nitrogen cycle with it being employed as a food preservative.[29,30] However, an increased level of nitrite in the environment may lead to significant toxic effects.[31] Nitrosamines, produced by the reaction of amines with nitrite, are carcinogenic. In humans, a high concentration of nitrite can cause the production of metheamoglobin by the oxidation of oxyheamoglobin which severely affects the oxygen carrying capacity of the blood leading to a medical condition termed "blue baby syndrome" or "methemoglobinemia".[32]

The novel work presented in this article focuses on the first time surface immobilization of an organic hybrid $[SiW_{10}O_{36}(PhPO)_2]^{4-}$ POM by employing layer by layer methodology using Ru(II) metallodendrimer and by entrapment into a conducting polypyrrole matrix. The novelty of this work is based upon this surface immobilization study being the first to have been undertaken with this organic hybrid POM. In addition, the POM's ability to effectively electrocatalytically reduce nitrite while in the immobilized state represents the first known report of such activity for this specific POM.

EXPERIMENTAL SECTION

Materials. The pentaerythritol based rhuthenium metallodendrimer $Ru_4C_{125}N_{24}H_{92}P_8F_{48}$ was synthesized and characterized by our group according to the literature.[33] $[TBA]_3K[SiW_{10}O_{36}(PhPO)_2]$ POM was received from Andrea Sartorel's group in the University of Padova, Italy. All other chemicals were of reagent grade and used as received unless stated otherwise. 20% PDDA, (poly-(diallyldimethylammonium chloride)), MW 20,000, was used to prepare 8% PDDA solution. Tetrabutylammonium hexafluorophosphate, Bu_4NPF_6, was recrystallized twice from ethanol before use. Molecular sieves of size 3 Å were used to dry acetonitrile. Alumina powders of bead sizes 0.05, 0.3, and 1.0 μm were purchased from CHI Instruments. Ultrapure water with a resistivity of 18.2 MΩ at 25 °C from Millipore purification system was used to prepare the electrolyte solutions. The electrolytes used for the electrochemical studies were of following compositions, 0.1 M Na_2SO_4 (pH 2.0−3.0), 0.1 M Na_2SO_4/20 mM CH_3COOH (pH 3.5−5.0), and 0.1 M Na_2SO_4/20 mM NaH_2PO_4 (pH 5.5−7.0). pH of these electrolytes was adjusted either with 0.1 M NaOH or 0.1 M H_2SO_4.

Instrumentation and Procedure. Electrochemical measurements were carried out on a CHI 660 potentiostat by employing a standard three electrode system with a glassy carbon working electrode (area = 0.0707 cm^2), a platinum wire auxiliary and a Ag/AgCl reference electrode in aqueous media. For nonaqueous solutions, the reference electrode was a silver wire in contact with 0.01 M $AgNO_3$ in 0.1 M solution of electrolyte (Ag/Ag^+). The glassy carbon working electrode was cleaned by polishing it with alumina powder of 1.0 0.3 and 0.05 μm grain sizes successively and rinsed with distilled water between each polishing step. Finally the electrode was sonicated for 10 min and washed with ethanol prior to use. Cleaning of ITO slides was carried out by immersing them in a 0.1 M H_2SO_4 for 12 h, the cleaned slides were then rinsed thoroughly with deionized water and dried by nitrogen gas. The voltammetric measurements were performed at ambient temperature. The working solutions were degassed with high purity nitrogen for 15−20 min prior to voltammetric measurements for the complete removal of dissolved oxygen.

Electrochemical impedance measurements were performed by cycling the bare and POM/Ru dendrimer coated electrode in an aqueous solution of 10 mM potassium ferrocyanide and 10 mM potassium ferricyanide in 0.1 M KCl. Experiments were carried out by employing an applied potential of 230 mV vs Ag/AgCl reference system and a frequency range of 100 to 100 000 Hz with signal amplitude of 0.005 V. The working solution was prepared freshly prior to use and stored in the dark.

Multilayer assemblies of SiW_{10} and the ruthenium(II) metallodendrimer prepared on ITO slides were investigated for their surface morphology by SEM imaging by employing Zeiss SUPRA 40VP, field emission-scanning electron microscopy (FE-SEM), by setting the acceleration voltages at 10 kV. Samples for the atomic force microscopy (AFM) were prepared and characterized using the same equipment and procedures as reported previously.[34,35]

High-resolution X-ray photoelectron spectra were recorded by using a Kratos AXIS instrument with a monochromatic Al Kα radiation of 1486.6 eV energy as the excitation source (10 mA, 15 kV). All the spectra were acquired with analyzer pass energy of 20 eV and 100 ms dwell time per step. The spectra were fitted with a Gaussian profile using standard procedure. Binding energy values were calibrated by employing the C 1s 284.80 eV. The atomic concentration of the substituent elements was quantified by subtracting the Shirley-type background. High resolution scans of each detected element were acquired for about 160 scans each.

SiW_{10}-Doped Polypyrrole Film Formation. The electrodeposition of polypyrrole films doped with the SiW_{10} POM onto clean glassy carbon working electrodes was conducted in accordance with the literature.[36] Films of different thicknesses were fabricated by employing a fixed potential of +0.65 V and through the deposition of varying charges, namely, 2, 5, and 10 mC. The regular increase in the deposited charge (C/columb) with the passage of time (T/second) points to the continuous accumulation of the POM within the growing polypyrrole film. The redox activity of the polymer modified electrodes was then investigated in 0.1 M Na_2SO_4 buffer pH 2.0.

Construction of POM/Ru-Dend-Based Multilayer Assemblies. The previously reported procedure based on the layer-by-layer technique was followed to construct the multilayer assemblies on the glassy carbon electrode.[37−39] The surface of the precleaned glassy carbon electrode was modified by immersing in an 8% aq. PDDA solution for 30 min (step 1). It was rinsed with ultrapure water to remove the unbound polymer before drying with nitrogen gas. This modified electrode was then immersed in a 0.5 mM solution of the SiW_{10} POM in acetonitrile for 20 min to form the anionic POM layer by the electrostatic attraction with the oppositely charged PDDA molecules (step 2). After a fixed time, the electrode was removed from the POM solution and dried again with nitrogen gas. This PDDA/POM modified electrode was then transferred to a 0.02 mM acetonitrile solution of ruthenium dendrimer for 20 min (step 3). The cationic charge on the dendrimer is the driving force behind the

DOI: 10.1021/am5017864
ACS Appl. Mater. Interfaces 2015, 7, 1046−1056

ready association with anionic POM. The step 2 and 3 were reiterated to build the 8 bilayers. The construction of the multilayer assembly was scrutinized by recording cyclic voltammograms after each bilayer deposition.

RESULTS AND DISCUSSION

The redox behavior of $[TBA]_3K[SiW_{10}O_{36}(PhPO)_2]$ POM, herein after referred to as (SiW_{10}), was investigated by employing cyclic voltammetry both in the solution and immobilized states.

Solution Redox Properties of $[TBA]_3K[SiW_{10}O_{36}(PhPO)_2]$. The Keggin type SiW_{10} POM, was found to be insoluble in aqueous media therefore its basic redox behavior was investigated in 0.1 M $TBAPF_6$/MeCN as explained by Figure 2. Three redox couples are apparent,

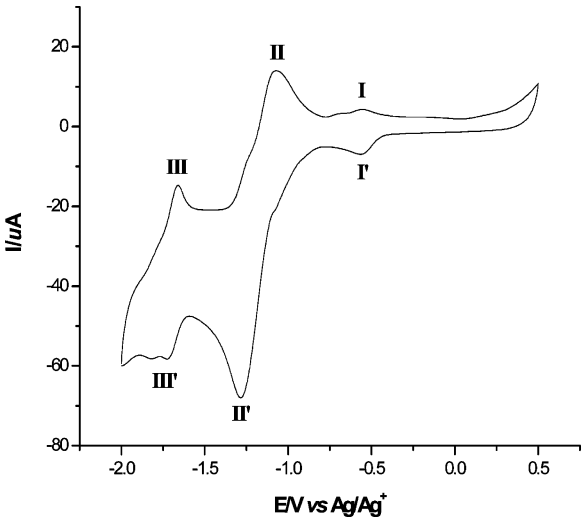

Figure 2. Cyclic voltammogram of a 2 mM SiW_{10} CH_3CN/Bu_4NPF_6 solution at GCE (nonaqueous Ag/Ag^+ electrode). Scan rate 100 mV/s. Initial scan direction is negative.

labeled as I/I′, II/II′, and III/III′ associated with the electrochemical activity of the POM's tungsten oxo framework. The first two of these couples with formal potential values of −0.556 and −1.177 V (vs Ag/Ag^+) were found to be monoelectronic in nature while the third process, $E_{1/2}$ = −1.691 V (vs Ag/Ag^+) is a bielectronic redox process. These observations are in compliance with the previously reported results.[40] This observed redox behavior for the POM corresponds to the following reactions:

$$[SiW_{10}O_{36}]^{4-} + 1e^- \leftrightharpoons [SiW_{10}O_{36}]^{5-} \quad (1)$$

$$[SiW_{10}O_{36}]^{5-} + 1e^- \leftrightharpoons [SiW_{10}O_{36}]^{6-} \quad (2)$$

$$[SiW_{10}O_{36}]^{6-} + 2e^- \leftrightharpoons [SiW_{10}O_{36}]^{8-} \quad (3)$$

Surface Immobilization of SiW_{10} POM. *SiW_{10}-Doped Polypyrrole Film.* Polypyrrole films doped with the SiW_{10} POM of varying thicknesses were fabricated on glassy carbon working electrodes by employing a potentiostatic method. The polymer modified electrodes were then investigated for their electrochemical behavior in 0.1 M Na_2SO_4 buffer pH 2.0. Figure 3 illustrates the voltammogram recorded for the SiW_{10}/polypyrrole composite film with an estimated surface coverage of 0.134 nmol·cm^{-2} calculated by employing the equation

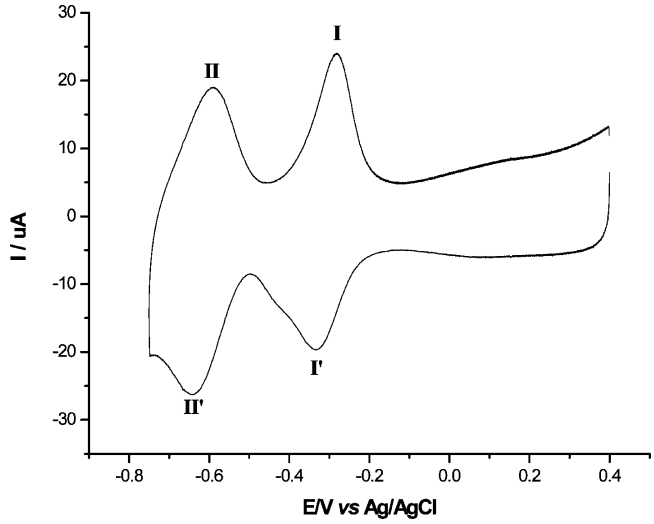

Figure 3. Cyclic voltammogram of a SiW_{10}/PPy hybrid film (Γ = 0.13 nmol cm^{-2}) on GCE cycled in 0.1 M Na_2SO_4 buffer (pH 2.0) (scan rate = 100 mV s^{-1}). The film was deposited at +0.65 V.

$$\Gamma = Q/nFA \quad (4)$$

where A represents the area of electrode, F is Faraday's constant, n is the number of electrons transferred, and Q is the charge passed during the redox process. What is readily seen is the presence of two well-behaved pH dependent bielectronic reversible redox processes, which are believed to be related to the electrochemical activity of the W−O framework of the POM. This observed redox pattern complies with the literature results.[41] These two redox processes labeled as I/I′ and II/II′ exhibit formal potential values of −0.306 and −0.614 V (vs Ag/AgCl) with corresponding peak to peak separation (ΔE) values of 50 and 51 mV, respectively. The deviation of ΔE values from the expected zero value for ideal thin film behavior might be attributed to the uncompensated resistance or some kinetic constraints. It is evident that the polymer bound POM shows well behaved redox behavior in aqueous buffer as compared to its behavior in organic media in the solution phase. This is probably due to the coupled electron/proton transfer phenomenon, a characteristic feature of POMs in acidic media where the effective densification of more than one monoelectronic processes leads to the generation of apparent multielectronic processes, supported by the protonation of the reduced species owing to their high basicity as has been explained previously in literature.[42−45] In this case, it appears that the two monoelectronic processes I and II observed for the solution behavior of SiW_{10} in Figure 2 have transformed into a single bielectronic process W−O (I) for the polymer bound POM. The significant anodic shifting of the reduction potentials is also a striking feature of the immobilized SiW_{10} POM in aqueous electrolyte which may be caused by the apparent interaction of the cations/H^+ favoring the stabilization of a more highly charged reduced species thereby resulting in the observed anodic shift. The observed redox activity of the POM within the polypyrole films can be summarized by eqs 5 and 6 below.

$$[SiW_{10}O_{36}]^{4-} + 2e^- + 2H^+ \leftrightharpoons [H_2SiW_{10}O_{36}]^{4-} \quad (5)$$

$$[H_2SiW_{10}O_{36}]^{4-} + 2e^- + 2H^+ \leftrightharpoons [H_4SiW_{10}O_{36}]^{4-} \quad (6)$$

DOI: 10.1021/am5017864
ACS Appl. Mater. Interfaces 2015, 7, 1046−1056

It was observed that cycling the polymer film through the second redox couple led to dramatic changes in the cyclic voltammogram, in that, the observed redox behavior was lost. This was probably due to cycling the film to potentials where reduction of the polymer backbone occurred thereby resulting in the leaching out of the POM from the film. In order to avoid this, potential cycling of the film was restricted to the narrow potential domain encompassing only the first tungsten-oxo based redox process. On subjecting the film to the "breaking-in" process, there is only a slight change in either the anodic or cathodic peak potentials (5−6 mV) and the peak currents (0.1−0.15 μA), between the initial (E_p^i) and final voltammetric scan (E_p^f) as explained by Figure 4, which indicates that the

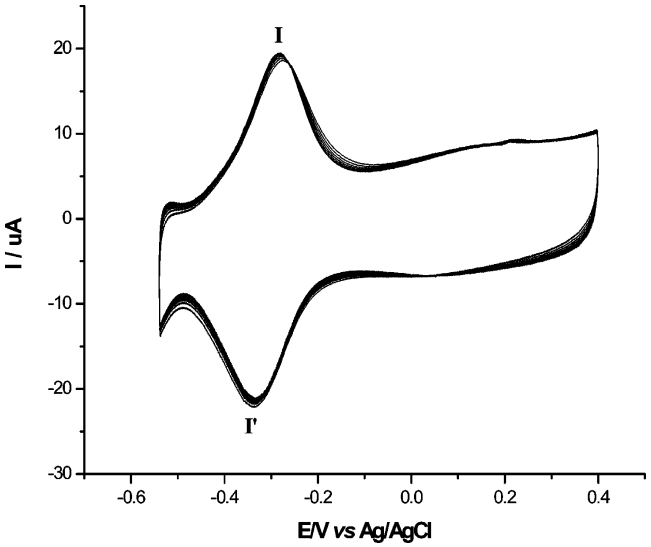

Figure 4. Breaking-in process of a SiW_{10}/PPy film (Γ = 0.13 nmol cm^{-2}) in 0.1 M Na_2SO_4 buffer (pH 2.0). Scan rate =100 $mV{\cdot}s^{-1}$.

redox cycling has essentially no effect on the film's morphology and these minor changes may attribute to the ingression of compensating counterions during the electrochemical reduction of the POM framework. When plotting against scan rates, peak potentials were found to be independent while associated peak currents exhibited a linear relationship with scan rate up to 2 V s^{-1} as seen in the Figures 5A and B, this being a characteristic of thin layer behavior. Peak splitting occurs at higher scan rate which ultimately causes the distorted peak symmetry. Supporting Information Table S1 summarizes the redox behavior of the SiW_{10}-polypyrrole hybrid films as a function of scan rate and surface coverage. It is clear from the data that with the increase in the film's thickness, the peak to peak separation values also increase which can be attributed to the augmentation of the hindrance of charge transfer within the thicker films.

The pH of the working electrolyte was found to have a noticeable effect on the redox activity of the SiW_{10} doped polypyrrole film. With increasing pH from pH 2 to 5, an expected negative shift in the peak potentials was observed as shown by the Supporting Information Figure S1(A). Supporting Information Figure S1(B) illustrates the relationship between the pH and the peak potentials for the first W−O redox couple with the measured slope indicating the addition of 2−3 protons for that electrochemical process.

SiW_{10}/Ru-Dendrimer Multilayer Assembly. Multilayer assemblies of SiW_{10} and the ruthenium(II) metallodendrimer

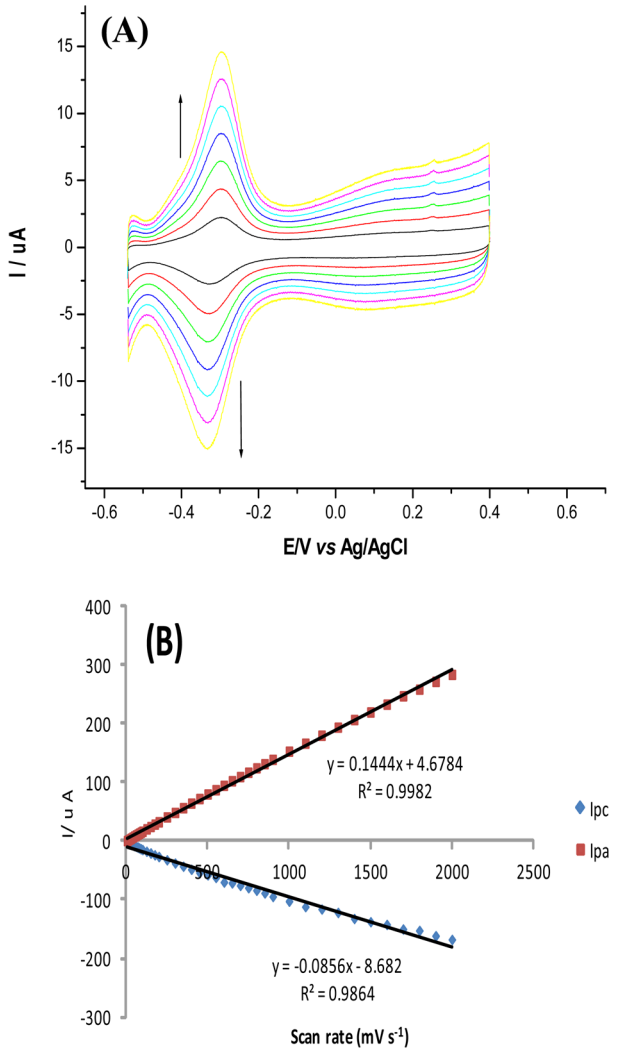

Figure 5. Overlayed cyclic voltammogrames of SiW_{10}/PPy hybrid film on GCE cycled in 0.1 M Na_2SO_4 pH 2.0 buffer at scan rates 10 (inner) to 70 (outer) mVs^{-1} (A). Graph between peak currents (I_{pc} and I_{pa}) and scan rate for a SiW_{10}/PPy film (Γ = 0.13 nmol cm^{-2}) (B).

were fabricated on precleaned glassy carbon working electrodes by following the procedure described in the Experimental Section. The deposition of the multilayer film was scrutinized by cyclic voltammetry by monitoring the redox activity of the assembled layer at both the negative (tungsten-oxo activity) and positive potential (ruthenium dendrimer activity) domains in pH 2.0 buffer, as shown in Figures 6 A and B, respectively. A gradual increase in the peak currents can be observed for the tungsten-oxo redox processes associated with the POM's framework and the Ru(III/II) metallodendrimer's redox process, with every successive deposited layer. These voltammograms were also found to be reproducible from layer to layer. Figure 6C shows the variation in the measured charges associated with the first and second tungsten-oxo redox processes with layer number. The linear variation can be indicative of regular and homogeneous growth of the multilayer assembly. The representative cyclic voltammogram of the resulting multilayer in pH 2.0 buffer (Supporting Information Figure S2) shows two well-defined bielectronic reversible tungsten-oxo redox couples with $E_{1/2}$ values of −0.32 and −0.66 V (vs Ag/AgCl), respectively, and a monoelectronic Ru(III/II) linked process with an $E_{1/2}$ of +1.05 V. The

DOI: 10.1021/am5017864
ACS Appl. Mater. Interfaces 2015, 7, 1046−1056

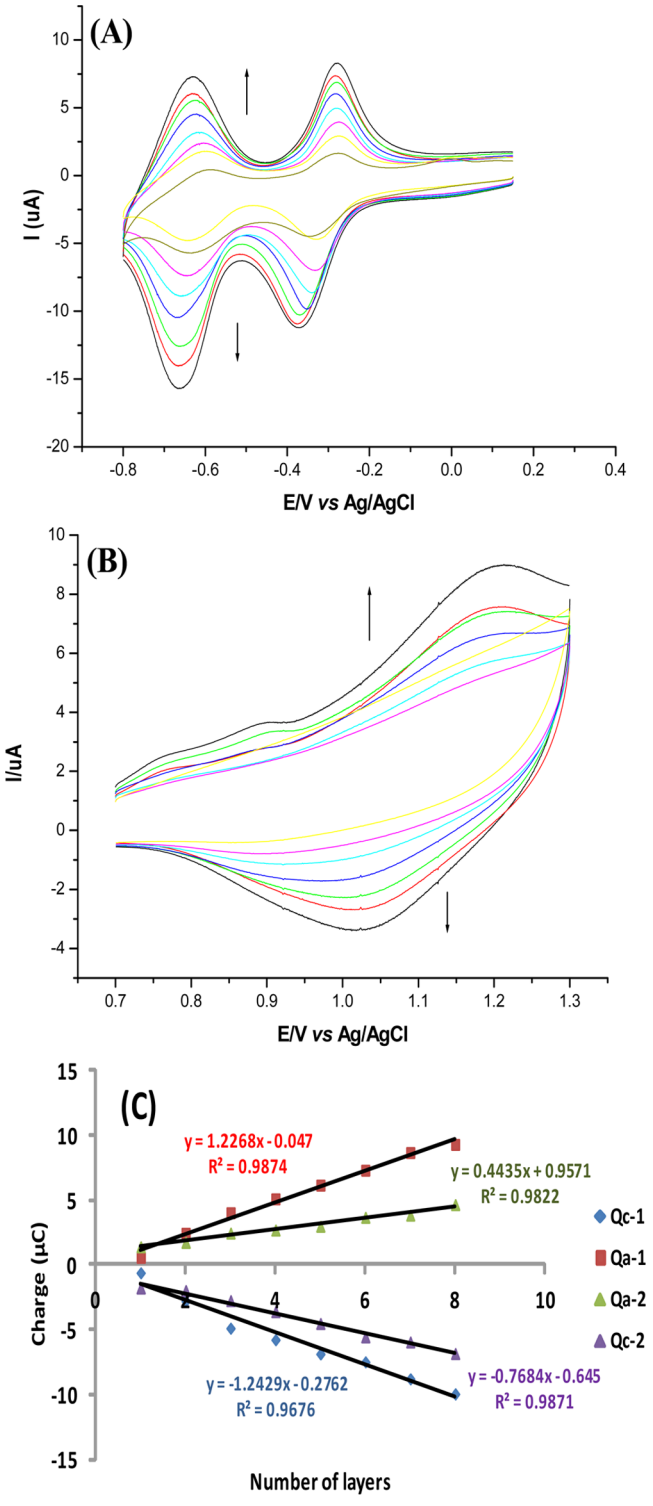

Figure 6. Cyclic voltammograms of the construction of a multilayer film (8 bilayers) having outer SiW_{10} POM layer in pH 2.0 buffer (0.1 M Na_2SO_4) on GCE (the scan rate was 0.1 V s^{-1}, scan direction negative) showing the tungsten-oxo redox activity of the POM (A) and Ru $^{III/II}$ process (B) indicating the increase in current with increasing layers. Plot of peak charges (Q_c and Q_a) versus layer number for the first (Q-1) and second (Q-2) tungsten-oxo redox process (C).

measured ΔE_p values for these processes were found to be 50, 35, and 90 mV, respectively, which is higher than the expected theoretical zero value for a surface confined species which may be attributed to the uncompensated resistance inside the cell or some sort of kinetic constraints. Furthermore, the value of Ip_a/Ip_c was close to 1 hence suggesting a reversible redox process.

The average surface coverage values of both Γ_{ox} and Γ_{red} were found to be 0.16 and 0.43 nmol cm^{-2} respectively, suggesting a monolayer coverage.[22] This is in accordance with the previously reported results by Wang and co-workers.[46] The scan rate study on the film revealed that the peak potentials linked to the W−O redox processes were independent of the scan rate up to 100 mVs^{-1}, while the peak currents varied in a linear fashion with scan rate as shown in Supporting Information Figure S2 B and C indicating a surface confined process.[47] Supporting Information Table S2 summarizes the electrochemical data for the second tungsten-oxo redox process. The values of full width at half-maximum ($fwhm_{ox}$) were 140 and 156 mV for the two tungsten-oxo redox processes, respectively. This deviation from the expected ideal value of 45.3 mV may be attributed to some sort of weak destabilizing interactions between the adsorbed redox active sites.[48]

The effect of pH of the supporting electrolyte on the redox behavior of the entrapped POM within the constructed multilayer can be observed by Supporting Information Figure S3 (A). It is evident from the voltammograms that with increasing pH, both W−O redox processes show a cathodic shift and a continuous decrease in their peak currents, suggesting a slow penetration of the cations toward the electrode so as to maintain charge neutrality.

Supporting Information Figure S3 (B) illustrates the relationship between the pH and the formal peak potentials for the second tungsten-oxo redox process. From the value of the observed shift i.e 60 (±0.5), the number of H^+ ions entered into this electrochemical process was calculated to be 2. This system is quite stable and reversible over a pH range from 0.0 to 8.0. The effect of the charge of the outermost layer on the electrochemical response of the POM based multilayer film was also scrutinized by recording the voltammogram after the adsorption of each cationic dendrimer layer as illustrated by Supporting Information Figure S4. What is readily seen is that the POM still shows its reversible redox behavior without any considerable change in the peak currents unlike the previously reported results where the POM's redox activity was masked by the cationic moiety.[49]

Electrochemical Impedance Spectroscopy (EIS). Electrochemical impedance spectroscopy (EIS) allows the evaluation of kinetic as well as diffusional components for electroactive surface confined electro-active systems. Impedance is actually the measure of the hindrance offered by multilayer assemblies to the diffusion of an electrochemically active probe, $[Fe(CN)_6]^{3-/4-}$ toward the underlying electrode surface. Figure 7 depicts the impedance plots of the ferri/ferrocyanide redox couple, at a bare glassy carbon electrode and at different stages during the construction of the SiW_{10} based multilayer system, with the applied potential being adjusted to the $E_{1/2}$ of the redox probe. It can be observed from the plots that as the number of layers deposited increases the redox process moves from being purely diffusion controlled to one which is primarily kinetically controlled, with an associated increase in the measured charge transfer resistance value (R_{ct}).

Quantitative interpretation of the impedance graph was performed by employing the appropriate equivalent Randles circuit and extracting the electrical parameters. The equivalent circuit comprises an electrolyte resistance, R_s in series with a

DOI: 10.1021/am5017864
ACS Appl. Mater. Interfaces 2015, 7, 1046−1056

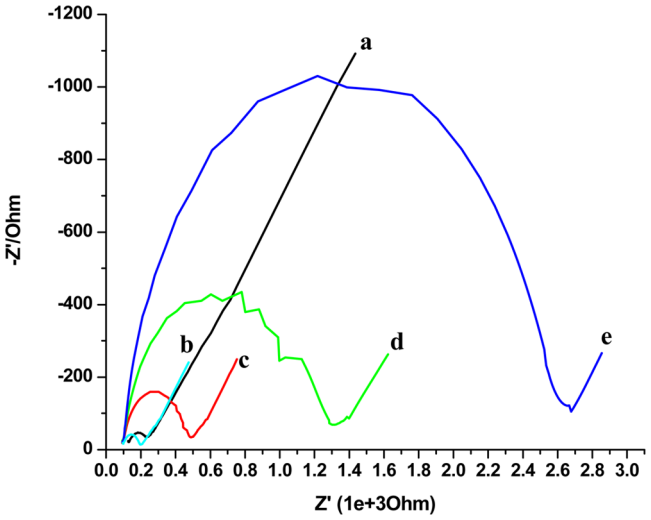

Figure 7. Impedance plots of the multilayer film with increasing layer number where (a) bare GCE, (b) GCE/PDDA, (c) GCE/PDDA/POM, (d) GCE/PDDA/POM/Ru dendrimer, and (e) GCE/PDDA/POM/Ru dendrimer/POM. Frequency range = 0.1 to 100000 Hz; signal amplitude = 0.005 V; applied potential = +0.23 V. Electrolyte: 10 mM $K_4[Fe(CN)_6]$/10 mM $K_3[Fe(CN)_6]$ in 0.1 M KCl.

parallel circuit of double layer capacitance C_{dl} and a charge transfer resistance R_{ct}, along with a diffusional branch, that is, Warburg impedance Z_W.[50−52] However, in this case, a constant phase element (CPE) was introduced into the equivalent circuit instead of C_{dl}, which defines the nonuniform distribution of the capacitance over the surface due to the amorphous nature of the glassy carbon working electrode. Supporting Information Figure S5A explains the switching behavior of the double layer capacitance. What is clearly seen is that the modification of the working electrode using PDDA as the base layer resulted in a 65% drop in C_{dl}. It was also observed that the deposition of the anionic POM caused a subsequent increase in C_{dl}. However, the extent of this effect diminishes as the number of layers increases suggesting a lesser influence of the thickness of multilayer on the C_{dl} value at the electrode/solution interface. A sharp increase in the Warburg element (Supporting Information Figure S5 B) was observed on the absorption of the first layer. The reason behind this effect is probably the increased surface area available for the charge transfer to/from the electrode. The R_{ct} values for the initial layers were smaller; however, the curve shows a direct relationship with the layer number from the third deposited layer as illustrated by the Supporting Information Figure S5C. This relatively different behavior of the multilayer assembly for the initial layers as compared to the subsequent ones suggests a less compact film at the initial stages of fabrication thereby allowing the redox probe to permeate the film through pinholes and defects for reaction at the underlying electrode. Table 1 illustrates the impact of the multilayer film's thickness on fitted values of the Randles circuit elements.

Permeability of Multilayer Systems. A thorough understanding of solute transport through thin films is important in describing the catalytic or inhibitory behavior of such films.[53] The permeability of the constructed multilayer assemblies toward anionic, that is, $[Fe(CN)_6]^{3-}$ and cationic, that is, $[Ru(NH_3)_6]^{3+}$ probe molecules has been investigated. $[Ru(NH_3)_6]^{3+}$ shows a well behaved monoelectronic redox process with an $E_{1/2}$ of −0.237 V (vs Ag/AgCl) while $[Fe(CN)_6]^{3-}$ shows a monoelectronic redox process with an $E_{1/2}$ of +0.282 V (vs Ag/AgCl). Supporting Information Figure S6 represents the redox behavior of $Fe(CN)_6^{4-/3-}$ probe at an electrode surface modified with the SiW_{10}/Dendrimer assembly comprised of 4 bilayers with an outer POM (S6 A) and outer dendrimer layer (S6 C). A slight reduction in peak currents linked with the redox activity of the probe can be observed with an associated increase in the peak to peak separation as compared to their behavior at the bare carbon electrode. This shows that the film still allows penetration of the redox probe to a greater extent. However, it does appear that the multilayer assembly consisted of 4 bilayers with an outer positively charged dendrimer layer appears to be slightly more permeable than a film having an outer negatively charged POM layer. This may be explained by the presence of attractive forces between the probe and the outer cationic layer. However, upon increasing the number of bilayers to 8, the permeability showed a substantial decrease but the redox activity of the probe can still be observed as explained by Supporting Information Figure S6B and D.

Table 1. Parameters Acquired from the Complex Impedence Spectra of the $(SiW_{10}/Ru\ Dendrimer)_n$ Multilayer Assemblies at GCE at +0.23 V in 10 mM $K_4[Fe(CN)_6]$/10 mM $K_3[Fe(CN)_6]$ in 0.1 M KCl by Fitting to Equivalent Circuit

layer no.	R_{ct} (KΩ)	C (μF cm^{-2})	W (Ω cm^2)
0	0.126	0.32	226
1	0.187	0.11	118
2	0.399	0.32	218
3	1.164	0.17	273
4	2.549	0.26	172

In contrast to ferricyanide, the electron transfer process for the $[Ru(NH_3)_6]^{+3}$ moiety was not affected drastically by the presence of the multilayer assembly as illustrated by the Supporting Information Figure S7 A-D. The reversibility of this redox couple was maintained with a very negligible alteration in the peak to peak separation value (ΔE) and peak currents suggesting that the films in general show greater permeability to the cationic probe. Stability study of the modified electrode showed that the multilayer assembly possessed a relatively good stability toward redox cycling, pH of the electrolyte and storage period as mentioned by Supporting Information Figure S8.

Surface Characterization. The morphology and composition of the immobilized films were determined by scanning electron microscopy, atomic force microscopy, and X-ray photoelectron spectroscopy.

Figure 8 shows the SEM images of the multilayer assembly consisted of 8 bilayers having an outer anionic POM (A), outer dendrimer moiety (B) and SiW_{10}-doped polypyrrole film (C). It may be seen from these images that the surfaces of the films are not smooth; the multilayer assembly exhibits a dendritic type structure whereas the POM entrapped polypyrrole film is granular in nature. Cross section images of the film with 8 bilayers and the POM-doped polymer film are shown in Supporting Information Figure S9. Viewed in cross-section, globular structures of varying sizes were seen in both films. The diameter of the globules seems to vary appreciably both within each film, and between the LBL and POM/polypyrrole film.

Variations in the surface morphology of the multilayer assemblies were also investigated by AFM in tapping mode. A series of topography and phase AFM images were obtained at each stage of the fabrication process. The topography images

DOI: 10.1021/am5017864
ACS Appl. Mater. Interfaces 2015, 7, 1046−1056

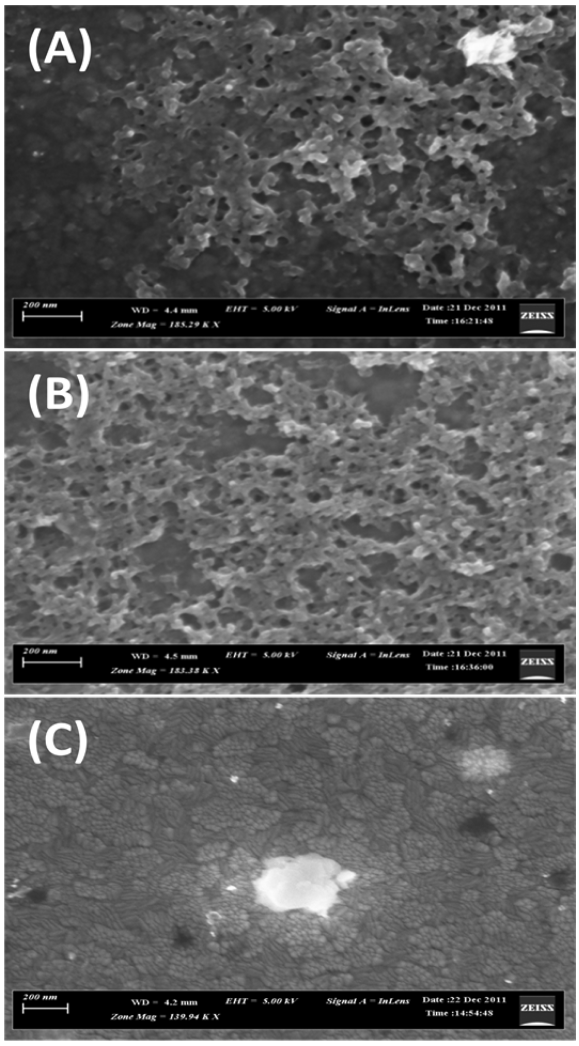

Figure 8. SEM images of multilayer film composed of 8 bilayers having outer POM (A) outer dendrimer moiety (B) and POM-doped polypyrrole film (C).

are presented in Figure 9. *Sq*, the mean root square surface roughness, was calculated from these topography images. From these data, the influence of the underlying ITO substrate on the polymer film morphology as successive layers are applied may be clearly seen. Upon deposition of the PDDA base layer onto the surface of the ITO substrate, a decrease in the root-mean-square height, *Sq* of the surface from 4.40 nm (Figure 9A) to 3.88 nm (Figure 9B) was observed. *Sq* was 3.88 nm after deposition of the first POM monlayer (Figure 9C), suggesting that the polymer layer was preferentially deposited in the valleys present on the ITO surface.

The influence of the ITO substrate's morphology could no longer be seen after 8 bilayers were deposited, as may be seen from Figure 9D and E. Globular structures were observed on the surfaces which were of similar shape and distribution for the films with different terminal moieties. However, *Sq* was slightly lower for the SiW_{10} terminal layer (Figure 9D) than for the Ru dendrimer terminal layer (Figure 9E) 11.6 vs 14.9 nm. Thus, it is suggested that the anionic POM filled the low lying valleys present in the underlying surface, whereas the cationic Dendrimer agglomerated on the surface resulting in higher *Sq* values. These observations are in agreement with previously reported data.[8] *Sq* for the SiW_{10}-doped polypyrrole doped hybrid film (Figure 9F) was 7.09 nm.

Little variation in phase contrast was seen for each sample analyzed, though appreciable differences in phase angle were observed between samples (AFM phase images are presented in Supporting Information, Figure S10). It is known that a wide range of phase contrasts may be observed between inhomogeneous regions on the same sample.[54] Recently, Raj et al.[55] have demonstrated that, for POM−polymer hybrid samples, hard POM entities appeared as well-defined bright (i.e., larger positive phase shift) spheres whereas softer polymer entities appeared as softer polymer materials are seen as darker (i.e., smaller phase shift) regions. Hence, the absence of phase variation within samples suggests that each surface consists solely of POM or RuDend, and the change in phase angle between samples suggests that each successive step in the multilayer deposition process resulted in the formation of an additional homogeneous monolayer.

X-ray photoelectron spectroscopy was exploited to elucidate the elemental composition of the multilayer assembly. XPS data confirmed the presence of Si (2.3%), Ru (0.8%), W (5.2%), C (56%), O (28.4%), and N (5.1%) within the multilayer film. Supporting Information Figure S11 illustrates the survey spectrum of the multilayer assembly. The presence of the anionic SiW_{10} layer was evident from the Si 2p signal with a binding energy at 101.7 eV, W 4f doublet at 35.4 and 37.4 eV for W $4f_{7/2}$ and W $4f_{5/2}$ levels respectively and P 2p corresponding to 132.7 eV (Supporting Information Figure S12). The presence of the pyridine based Ru-dendrimer layer was confirmed by the N 1s peak associated with the binding energy of 400 eV and a doublet linked to Ru at 281.1 and 285.2 eV for Ru $3d_{5/2}$ and Ru $3d_{3/2}$ levels (Supporting Information Figure S12). For the SiW_{10} hybrid polypyrrole film as illustrated by the Supporting Information figure S13, in addition to the anionic POM, the presence of the polymeric component of the film was evident by the C 1s and N 1s characteristic spectra. The C 1s spectrum can be differentiated mainly into peaks associated with the C═C (284.8 eV) and C−O/C−N (286.6 eV) while the N 1s peak with the binding energy of 400 eV corresponds to the C−N bond and the peak at 401.7 eV corresponds to the ammonium part (N^+). N/N^+ ratio was used to calculate the dopant level of the hybrid film which was found to be 0.6.

Preliminary Electrocatalytic Properties. Polyoxometalates have been used as mediator for the electrocatalysis of nitrite in their reduced forms. Unfortunately, most of the previously reported POM based assemblies operated only at very low pH, that is, 0−2 because of the instability of the POMs over a large pH range which limits their practical application.[56] However, SiW_{10} POM exhibited a good stability over a wide pH domain which can make it a suitable electrochemical sensor for the detection nitrite in real samples at their own pH environment, for example, soil, wood pulp, tap water, industrial effluent, and meat industry.

The fabricated multilayer assembly was also investigated for its electrocatalytic efficiency toward the reduction of nitrite. Figure 10a shows the overlay of cyclic voltammograms recorded for the SiW_{10} POM based layer-by-layer assembly, which is comprised of 8 alternating monolayers of SiW_{10} and $[RuDen](PF_6)_8$, in pH 4.5 buffer in both the absence and presence of varying concentrations of nitrite. It is quite clear that the cathodic peak current related to the second tungsten-oxo redox process is greatly increased with the addition of

DOI: 10.1021/am5017864
ACS Appl. Mater. Interfaces 2015, 7, 1046−1056

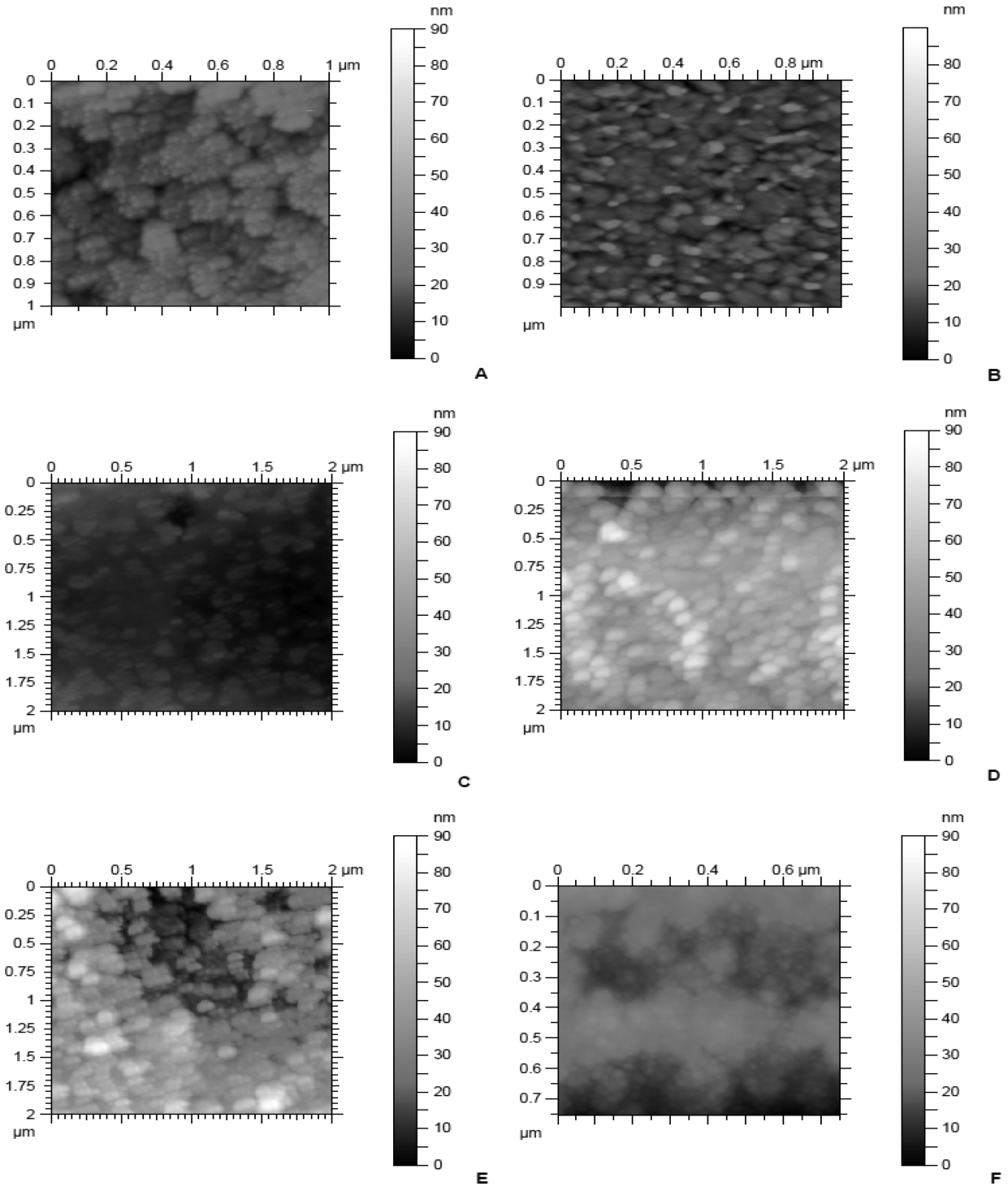

Figure 9. AFM topographic images of (A) clean ITO slide, (B) ITO/PDDA, (C) ITO/PDDA/POM (monolayer), (D) ITO/PDDA/POM composed of 8 bilayers with outer POM layer, (E) ITO/PDDA/POM composed of 8 bilayers with outer dendrimer layer, and (F) POM-doped polypyrrole film.

nitrite along with an associated current decrease in its anodic counterpart. However, the peak currents for the first redox process remain almost unaffected indicating that only the reduced form of SiW_{10} POM assists in the electro-reduction of the nitrite at pH 4.5.

For comparison, the electrochemical reduction of nitrite at bare glassy carbon electrode was also investigated under the same experimental conditions but no obvious interaction was observed suggesting the inactivity of bare electrode toward the nitrite at the respective pH (Figure 10b). Quantitative catalytic behavior of the modified electrode can be assessed by calculating the electrochemical catalytic efficiency by employing the expression

$$\mathrm{CAT} = \{[I_{(\mathrm{POM}+\mathrm{NO_2^-})} - I_{(\mathrm{POM})}]/I_{(\mathrm{POM})}\} \times 100 \quad (7)$$

where $I_{(\mathrm{POM}+\mathrm{NO_2^-})}$ is the peak current response of the POM multilayer in the presence of NO_2^- and $I_{(\mathrm{POM})}$ is the peak

DOI: 10.1021/am5017864
ACS Appl. Mater. Interfaces 2015, 7, 1046−1056

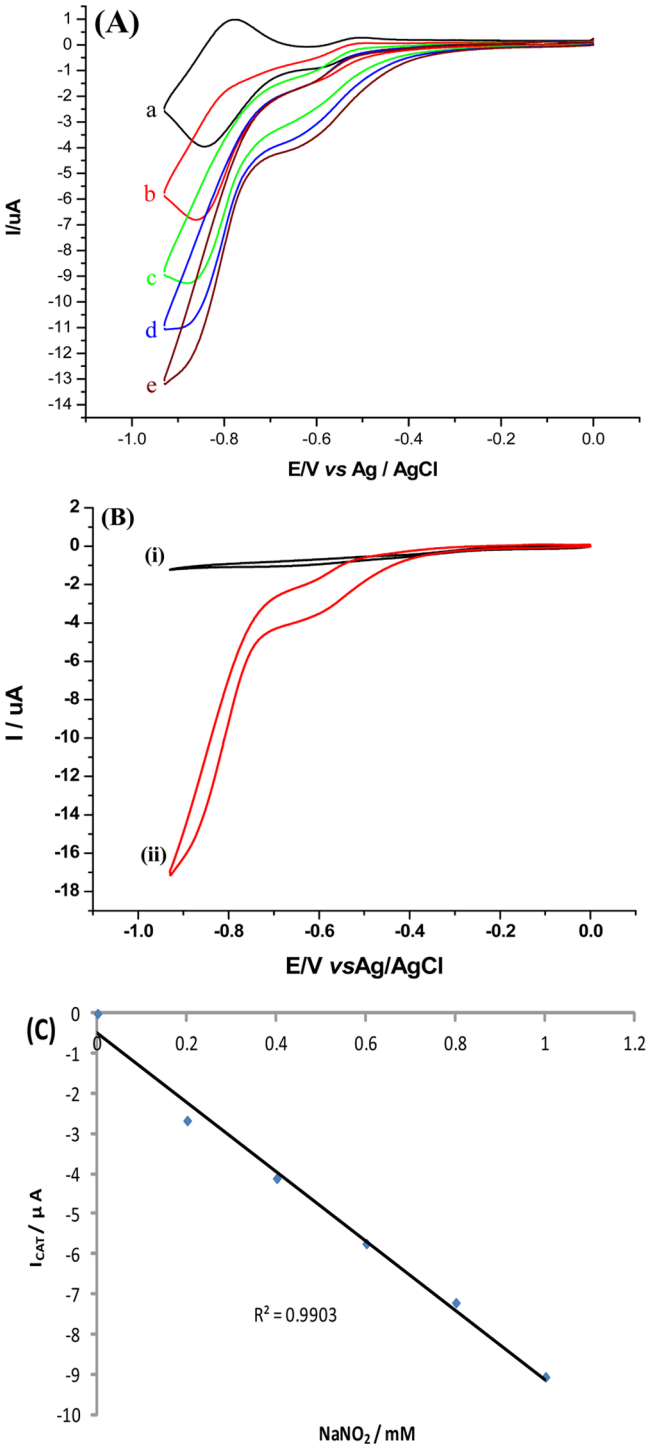

Figure 10. Cyclic voltammograms of GCE coated with SiW_{10}/Ru dend based multilayer assembly composed of 4 bilayers in absence and presence of $NaNO_2$ up to 1 mM in pH 4.5 buffer where (a) 0.0, (b) 0.2, (c) 0.4, (d) 0.6, and (e) 0.8 mM NO_2^- (A) at a scan rate of 5 mV s^{-1}. (B) Comparison of the cyclic voltammograms for bare glassy carbon electrode (i) and 4 bilayer multilayer assembly at 1.0 mM NO_2^{-1} and (C) catalytic current (I_{CAT}) versus concentration of nitrite for the electrocatalysis of nitrite at GCE modified with SiW_{10}/Ru dend based multilayer assembly.

current of multilayer in the absence of NO_2^- ions. From the equation the calculated catalytic efficiency was found to be increased from 45% for 0.2 mM NO_2^- to 230% for 1 mM NO_2^-.

Figure 10c shows a direct relationship between the measured catalytic cathodic currents and the concentration of NO_2^- up to 1.0 mM, with a correlation coefficient of 0.990 and a sensitivity of 122 (±0.4) mA·M^{-1}·cm^{-2}, which is much higher than most of the previously POM-based electrocatalytic systems.[57] For instance Cheng and co-worker[58] reported the electrocatalysis of nitrite by employing a $P_2W_{18}O_{62}^{-6}$/polyamidoamine dendrimer multilayer assembly at pH 1.1 showing a sensitivity of 2.8 mA·M^{-1}·cm^{-2}. Fernandes et al.[59] fabricated the layer by layer assembly based on $[SiW_{11}Fe(H_2O)O_{39}]$/PEI which catalyzed the electro-reduction of nitrite at pH 4.0 with a sensitivity of 6 mA·M^{-1}·cm^{-2}.

CONCLUSION

An organic functionalized POM was successfully immobilized on glassy carbon electrode surface by exploiting layer-by-layer and conducting polymer entrapment techniques. The fabricated assemblies were found to be well organized and reproducible. However, it was found that the multilayer films show more stability toward a wide pH range and redox cycling even in more negative potential domain. Cyclic voltammetry and AC impedance studies showed the regular growth of the multilayer assembly. Most importantly, it was observed that the presence of cationic dendrimer in case of multilayer assembly does not have any masking effect on the redox activity of POM. Multilayer films showed substantial permeability toward redox probes, furthermore the number of layers and the nature of outermost layer within the assemblies impacted upon the films' permeability. The surface features of the films were investigated by employing a set of advanced surface characterization tools including AFM and SEM. XPS confirms the presence of constituent elements within the films. All these techniques provide the consistent results. Additionally the multilayer assembly also displayed good electrocatalytic ability toward the reduction of nitrite.

ASSOCIATED CONTENT

Supporting Information

Effect of electrolyte's pH on the redox behavior of SiW_{10}/polypyrrole hybrid film, electrochemical behavior of the SiW_{10}/Ru dendrimer multilayer assembly with outer dendrimer moiety, dependency of interfacial and kinetic parameters, that is, C_{dl}, Z_w, and R_{ct} on the number of deposited layers, permeability of multilayer assembly, stability study of the multilayer assembly, AFM topography images and XPS spectra of POM/Polypyyrole and multilayer assemblies. This material is available free of charge via the Internet at http://pubs.acs.org.

AUTHOR INFORMATION

Corresponding Author

*Fax: (+)353 42 933 1163. E-mail: tim.mccormac@dkit.ie.

Notes

The authors declare no competing financial interest.

ACKNOWLEDGMENTS

The authors would like to acknowledge Dundalk Institute of Technology for financial support and the research team of Prof Marcella Bonchio form the University of Padova, Italy, for kind donation of the $TBA_3K[SiW_{10}O_{36}(PhPO)_2]$ POM. The AFM and XPS work was conducted under the framework of the INSPIRE programme, funded by the Irish Government's

DOI: 10.1021/am5017864
ACS Appl. Mater. Interfaces 2015, 7, 1046−1056

Programme for Research in Third Level Institutions, Cycle 4, National Development Plan 2007-2013.

REFERENCES

(1) Pope, M. T. *Heteropoly and Isopoly Oxometalates*, Inorganic Chemistry Concept, Vol. *8*; Springer-Verlag: NewYork, 1983.

(2) Pope, M. T.; Muller, A. *Polyoxometalates Chemistry, From Topology via Self Assembly to Applications*, 1st ed.; Kluwer Academic Publishers: Dordrecht, the Netherlands, 2001.

(3) Yamase, T.; Pope, M. T. *Polyoxometalates Chemistry for Nano-Composite Design*, 1st ed.; Kluwer Academic, Plenum Publishers: New York, 2002.

(4) Pope, M. T. *Comprehensive Coordination Chemistry II*, Vol. *4*; McCleverty, J. A., Meyer, T. J., Eds.; Elsevier: Oxford, U.K., 2004; pp 635−678.

(5) Borras-Almenar, J. J.; Coronado, E.; Muller, A.; Pope, M. T. *Polyoxometalate Molecular Science*, Vol. *98*; Kluwer: Dordrecht, the Netherlands, 2003.

(6) Hill, C. L. *Comprehensive Coordination Chemistry II*, Vol. *4*; McCleverty, J. A., Meyer, T. J., Eds.; Elsevier: Oxford, U.K., 2004; pp 679−759.

(7) Lopez, X.; Carbo, J.; Bo, C.; Poblet, J. M. Structure, Properties and Reactivity of Polyoxometalates: A Theoretical Perspective. *Chem. Soc. Rev.* **2012**, *41*, 7537−7571.

(8) Zynek, M.; Serantoni, M.; Beloshapkin, S.; Dempsey, E.; McCormac, T. Electrochemical and Surface Properties of Multilayer Films Based on a Ru^{2+} Metallodendrimer and the Mixed Addenda Dawson Heteropolyanion. *Electroanalysis* **2007**, *19*, 681−689.

(9) McCormac, T.; Bidan, G.; Fabre, B. Role of pH and of the Transition Metal for the Electrocatalytic Reduction of Nitrite with Transition Metal-Substituted Dawson Type Heteropolyanions. *J. Electroanal. Chem.* **1997**, *427*, 155−159.

(10) Miras, H. N.; Yan, J.; Long, D. L.; Cronin, L. Engineering Polyoxometalates with Emergent Properties. *Chem. Soc. Rev.* **2012**, *41*, 7403−7430.

(11) Rhule, J. T.; Hill, C. L.; Judd, D. A. Polyoxometalates in Medicine. *Chem. Rev.* **1998**, *98*, 327−358.

(12) Alizadeh, M. H.; Salimi, A. R. Density Functional Theory and Hartree−Fock Studies: Geometry, Vibrational Frequencies and Electronic Properties of Anderson-type Heteropolyanion, $[XM_6O_{24}]^{n-}$ (X = Te^{VI}, I^{VII} and M = Mo, W) and $[Sb^{V}W_6O_{24}]^{7-}$. *Spectrochim. Acta, Part A* **2006**, *65*, 1104−1111.

(13) Gouzerh, P.; Proust, A. Main-Group Element, Organic, and Organometallic Derivatives of Polyoxometalates. *Chem. Rev.* **1998**, *98*, 77−112.

(14) Mayer, C. R.; Herson, P.; Thouvenot, R. Organic−Inorganic Hybrids Based on Polyoxometalates. 5. 1 Synthesis and Structural Characterization of Bis(organophosphoryl)decatungstosilicates $[\gamma\text{-}SiW_{10}O_{36}(RPO)_2]^{4-}$. *Inorg. Chem.* **1999**, *38*, 6152−6158.

(15) Berardi, S.; Bonchio, M.; Carraro, M.; Conte, V.; Sartorel, A.; Scorrano, G. Fast Catalytic Epoxidation with H_2O_2 and $\gamma\text{-}SiW_{10}O_{36}(PhPO)_2]^{4-}$ in Ionic Liquids under Microwave Irradiation. *J. Org. Chem.* **2007**, *72*, 8954−8957.

(16) Carraro, M.; Sandei, L.; Sartorel, A.; Scorrano, G.; Bonchio, M. Hybrid Polyoxotungstates as Second-Generation POM-Based Catalysts for Microwave-Assisted H_2O_2 Activation. *Org. Lett.* **2006**, *8*, 3671−3674.

(17) Ulman, A. *An Introduction to Ultra Thin Organic Films: From Langmuir-Blodgett to Self-Assembly*, 1st ed.; Academic Press: New York, 1991.

(18) Shimidzu, T.; Ohtani, A.; Aiba, M.; Honda, K. Electrochromism of a Conducting Polypyrrole−Phosphotungstate Composite Electrode. *J. Chem. Soc., Faraday Trans. 1* **1988**, *84*, 3941−3949.

(19) Keita, B.; Bouaziz, D.; Nadjo, L. Strategies for Entrapping Oxometalates in Polymeric Matrices, Example of Polyaniline as the Matrix. *J. Electroanal. Chem.* **1988**, *255*, 303−313.

(20) Lapkowski, M.; Bidan, G.; Fournier, M. Synthesis of Polypyrrole and Polythiophene in Aqueous Solution of Keggin-Type Structure Heteropolyanions. *Synth. Met.* **1991**, *41*, 407−410.

(21) Bao, Y.; Bi, L.; Wu, L.; Mal, S. S.; Kortz, U. Preparation and Characterisation of Langmuir−Blodgett Films of Wheel-Shaped Cu-20 Tungstophosphate and DODA by two Different Strategies. *Langmuir* **2009**, *25*, 13000−13006.

(22) Wang, Y. H.; Hu, C. W. Layer-by-Layer Self Assembly of Dye-Polyoxometalate Multilayer Composite Films and their Fluorescent Properties. *Thin Solid Films* **2005**, *476*, 84−91.

(23) Jiang, M.; Wang, E.; Wang, X. L.; Wu, A. G.; Kang, Z. H.; Lian, S. Y.; Xu, L.; Li, Z. Self-Assembly of Lacunary Dawson Type Polyoxometalates and Poly(Allylamine Hydrochloride) Multilayer Films: Photoluminescent and Electrochemical Behaviour. *Appl. Surf. Sci.* **2005**, *242*, 199−206.

(24) Zhai, S. Y.; Gong, S. Y.; Jiang, J. U.; Dong, S. J.; Li, J. H. Assembly of Multilayer Films Containing Iron (III)-Substituted Dawson-type Heteropolyanions and Its Electrocatalytic Properties: Cyclic Voltammetry, Electrochemical Impedence Spectroscopy, and UV−vis Spectrometry. *Anal. Chim. Acta* **2003**, *486*, 85−92.

(25) Zhang, X.; Chen, H.; Zhang, H. Y. Layer-by-Layer Assembly: From Conventional to Unconventional Methods. *Chem. Commun.* **2007**, *14*, 1395−1405.

(26) Cheng, L.; Pacey, G. E.; Cox, J. A. Preparation and Electrochemical Applications of a Multilayer Nanocomposite Consisting of Phosphomolybdate and Poly(Amidoamine). *Electrochim. Acta* **2001**, *46*, 4223−4228.

(27) Liu, S.; Kurth, D. G.; Bredenkotter, B.; Volkmer, D. The Structure of Self-Assembled Multilayers with Polyoxometalate Nanoclusters. *J. Am. Chem. Soc.* **2002**, *124*, 12279−12287.

(28) Cheng, L.; Cox, J. A. Nanocomposite Multilayer Film of a Ruthenium Metallodendrimer and a Dawson-Type Polyoxometalate as a Bifunctional Electrocatalyst. *Chem. Mater.* **2002**, *14*, 6−8.

(29) Cammack, R.; Joannou, C. L.; Cui, X.; Martinez, C.; Maraj, S.; Hughes, M. Nitrite and Nitrosyl Compounds in Food Preservation. *Biochim. Biophys. Acta* **1999**, *1411*, 475−488.

(30) Heaton, K. M.; Cornforth, D. P.; Moiseev, I. V.; Egbert, W. R.; Carpenter, C. E. Minimum Sodium Nitrite Levels for Pinking of Various Cooked Meats as Related to Use of Direct or indirect-Dried Soy Isolates in Poultry Rolls. *Meat Sci.* **2000**, *55*, 321−329.

(31) Jensen, F. Nitrite Disrupts Multiple Physiological Functions in Aquatic Animals. *Comp. Biochem. Physiol., Part A: Mol. Integr. Physiol.* **2003**, *135*, 9−24.

(32) Yang, H.; Cheng, H. Controlling Nitrite Level in Drinking Water by Chlorination and Chloramination. *Sep. Purif. Methods* **2007**, *56*, 392−396.

(33) Constable, E. C.; Housecroft, C. E.; Cattalini, M.; Phillips, D. Pentaerythritol-Based Metallodendrimers. *New J. Chem.* **1998**, *22*, 193−200.

(34) Anwar, N.; Sartorel, A.; Yaqub, M.; Wearen, K.; Laffir, F.; Armstrong, G.; Dickinson, C.; Bonchio, M.; McCormac, T. Surface immobilization of a tetra-Ruthenium Substituted Polyoxometalate Water Oxidation Catalyst Through the Employment of Conducting Polypyrrole and the Layer-by-Layer (LBL) Technique. *ACS Appl. Mater. Interfaces* **2014**, *6*, 8022−8031.

(35) Naseer, R.; Mal, S. S.; Ibrahim, M.; Kortz, U.; Armstrong, G.; Laffir, F.; Dickinson, C.; Vagin, M.; McCormac, T. Redox, Surface and Electrochemical Properties of Layer-by-layer Films Based Upon Fe(III)-Substituted Crown Polyoxometalate $[P_8W_{48}O_{184}Fe_{16}(OH)_{28}(H_2O)_4]^{20-}$. *Electrochim. Acta* **2014**, *134*, 450−458.

(36) McCormac, T.; Farrell, D.; Drennan, D.; Bidan, G. Immobilisation of a Series of Dawson Type Heteropolyanions. *Electroanalysis* **2001**, *13*, 836−842.

(37) Neumann, R. Activation of Molecular Oxygen, Polyoxometalates, and Liquid-Phase Catalytic Oxidation. *Inorg. Chem.* **2010**, *49*, 3594−3601.

(38) Douvas, A.; Makarona, E.; Glezos, N.; Argitis, P.; Mielczarski, J.; Mielczarski, E. Polyoxometalate-Based Layered Structures for Charge Transport Control in Molecular Devices. *ACS Nano* **2008**, *2*, 733−742.

DOI: 10.1021/am5017864
ACS Appl. Mater. Interfaces 2015, 7, 1046−1056

(39) Anwar, N.; McCormac, T.; Compain, J. D.; Mialane, P.; Dolbecq, A.; Laffir, F. Surface Immobilisation of the Sandwich Type $Na_{14}[Fe_4(Ox)_4(H_2O)_2(SbW_9O_{33})_2]\cdot 60H_2O$ Polyoxometalate. *Electrochim. Acta* **2012**, *59*, 1−7.
(40) Perkins, L. M. Organic−Inorganic Hybrid Materials: New Functionalised Polyoxotungstates. PhD. Thesis, University of Birmingham, Birmingham, U.K., 2009.
(41) Canny, J.; Teze, A.; Thouvenot, R.; Herve, G. Disubstituted Tungstosilicates. 1. Synthesis, Stability and Structure of Lacunary Precursor Polyanion γ-$SiW_{10}O_{36}^{8-}$. *Inorg. Chem.* **1986**, *25*, 2114−2119.
(42) Wu, H. Contribution of the Chemistry of Phosphomolybdic Acids, Phosphotungstic Acids and Allied Substances. *J. Biol. Chem.* **1920**, *43*, 189−220.
(43) Pope, M. T.; Varga, G. M.; Heteropoly Blues, I. Reduction Stoichiometries and Reduction Potentials of Some 12-Tungstates. *Inorg. Chem.* **1966**, *5*, 1249−1254.
(44) Pope, M. T.; Papaconstantinou, E. Heteropoly Blues. II. Reduction of 2:18-Tungstates. *Inorg. Chem.* **1967**, *6*, 1147−1152.
(45) Keita, B.; Nadjo, L. New aspects of the Electrochemistry of Heteropolyacids Part IV. Acidity Dependent Cyclic Voltammetric Behaviour of Phosphotungstic and Silicotungstic Heteropolyanions in Water and *N*,*N*-Dimethylformamide. *J. Electroanal. Chem.* **1987**, *227*, 77−98.
(46) Wang, B.; Vyas, R. N.; Shaik, S. Preparation Parameter Development for Layer-by-Layer Assembly of Keggin-Type Polyoxometalates. *Langmuir* **2007**, *23*, 11120−11126.
(47) Kuhn, A.; Anson, F. C. Adsorption of Monolayers of $P_2Mo_{18}O_{62}^{6-}$ and Deposition of Multiple Layers of $Os(bpy)_3^{2+}$-$P_2Mo_{18}O_{62}^{6-}$ on Electrode Surfaces. *Langmuir* **1996**, *12*, 5481−5488.
(48) Zhang, Y. Q.; Wang, K. Z.; Gao, L. H. Electrostatically Self-Assembled Multilayer Film Formed by a Novel Ruthenium (II) Complex and $Nd(SiW_9Mo_2O_{39})_2^{13-}$. *Colloids Surf., A* **2005**, *257*, 391−394.
(49) Anwar, N.; Vagin, M.; Naseer, R.; Imar, S. Redox Switching of Polyoxometalate-Methylene Blue-Based Layer-by-Layer Films. *Langmuir* **2012**, *28*, 5480−5488.
(50) Zhai, S.; Gong, S.; Jiang, J.; Dong, S.; Li, J. Assembly of Multilayer Films Containing Iron(III)-Substituted Dawson-Type Heteropolyanions and its Electrocatalytic Properties: Cyclic Voltammetry, Electrochemical Impedance Spectroscopy, and UV−vis Spectrometry. *Anal. Chim. Acta* **2003**, *486*, 85−92.
(51) Cheng, Z.; Cheng, L.; Gao, Q.; Dong, S.; Yang, X. Characterization of Organic−Inorganic Multilayer Films by Cyclic Voltammetry, UV−vis Spectrometry, X-ray Photoelectron Spectroscopy, Small-Angle X-ray Diffraction and Electrochemical Impedance Spectroscopy. *J. Mater. Chem.* **2002**, *12*, 1724−1729.
(52) Yang, G.; Guo, H.; Wang, M.; Huang, M.; Chen, H.; Liu, B.; Dong, S. Assembly of 12-Tungstosilicic Acid and 4-Aminobenzo-15-crown-5 Ether Based on the Electrostatic Attraction through Bridging of Oxonium ions on Different Substrates. *J. Electroanal. Chem.* **2007**, *600*, 318−324.
(53) Ikeda, T.; Schmehl, R.; Danisevich, P.; Willman, K.; Murray, R. W. Permeation of Electroactive Solutes through Ultrathin Polymeric Films on Electrode Surfaces. *J. Am. Chem. Soc.* **1982**, *104*, 2683−2691.
(54) James, P. J.; Antognozzi, M.; Tamayo, J.; McMaster, T. J.; Newton, J. M.; Miles, M. J. Interpretation of Contrast in Tapping Mode AFM and Shear Forces Microscopy. A Study of Nafion. *Langmuir* **2001**, *17*, 349−360.
(55) Raj, G.; Swalus, C.; Guillet, A.; Devillers, M.; Nysten, B.; Gaigneaux, E. M. Supramolecular Organization in Organic−Inorganic Heterogeneous Hybrid Catalysts Formed from Polyoxometalate and Poly(Ampholyte) Polymer. *Langmuir* **2013**, *29*, 4388−4395.
(56) Ammam, M. Polyoxometalates: Formation, Structures, Principal Properties, Main Deposition Methods and Application in Sensing. *J. Mater. Chem. A* **2013**, *1*, 6291−6312.
(57) Casella, I. G.; Contursi, M. Electrochemical and Spectroscopic Characterization of a Tungsten Electrode as a Sensitive Amperometric Sensor of Small Inorganic Ions. *Electrochim. Acta* **2005**, *50*, 4146−4154.
(58) Cheng, L.; Cox, J. A. Preparation of Multilayered Nanocomposites of Polyoxometalates and Poly(Amidoamine) Dendrimers. *Electrochem. Commun.* **2001**, *3*, 285−289.
(59) Fernandes, D. M.; Carapuca, H. M.; Brett, C. M. A.; Cavaleiro, A. M. V. Electrochemical Behaviour of Self-assembly Multilayer Films Based on Iron-Substituted α-Keggin Polyoxotungstates. *Thin Solid Films* **2010**, *518*, 5881−5888.

DOI: 10.1021/am5017864
ACS Appl. Mater. Interfaces 2015, 7, 1046−1056